CONSTRUCTAL COOLING CHANNELS: APPLICATION TO HEAT TRANSFER IN MICRO-CHANNEL HEAT SINKS

Bello-Ochende, T[1]. and Meyer, J. P[2].
Department of Mechanical and Aeronautical Engineering
University of Pretoria, 0002, Pretoria
South Africa
tbochende@up.ac.za[1] and josua.meyer@up.ac.za[2]

ABSTRACT

This paper reports on the geometric optimisation of a three-dimensional micro-channel heat sink. Two types of micro-channel heat sink configurations were studied. In both cases, the objective was to maximise the global thermal conductance subject to a fixed volume, high conducting material and a fixed pressure drop. In the first configuration, the micro-channel was completely embedded inside a high conducting material and numerical simulations were carried out on a unit cell with volume ranging from 0.1 to 0.9 mm^3 and pressure drop between 10 and 75 kPa. The axial length of the micro-channel heat sink was fixed at 10 mm. The cross-sectional area of the micro-channel heat sink was free to morph with respect to the degrees of freedom provided by the aspect ratio and the solid volume fraction. The effects of the total solid volume fraction and the pressure drop on the aspect ratio, channel hydraulic diameter and peak temperature were investigated. In the second configuration the micro-channels were embedded inside a high conducting material, except that the top was covered with an insulating material. The whole configuration was allowed to morph with respect to all the degrees of freedom. Similar but dimensionless numerical simulations were carried out on this configuration and the numerical optimisation results were reported. In the first configuration numerical results show that the degrees of freedom have a strong effect on the peak temperature and the maximum thermal conductance. The optimal geometric characteristics (aspect ratio and the optimal channel shape) are reported and compared with those obtained from approximate relationships using scale analysis. For this configuration, the predicted trends are found to be in good agreement with the predicted results. In the second configuration, a test case on an actual micro-channel heat sink shows a reduction of about 8% in global thermal resistance.

Keywords: Constructal, micro-channel heat sinks, conductance, optimal geometry, conjugate

1. INTRODUCTION

The quest for better designs for the cooling of heat-generating devices has been a driving force for innovation and new fundamentals for heat transfer engineering and science. Micro-channels are currently at the forefront of cooling technologies, because of the difficulties of meeting with air-cooling techniques the cooling needs of devices with high heat flux (projected to exceed 100 W/cm^2)[1-3]. In modern heat transfer, the challenge is how to cool, manufacture, decrease cost and optimise performance. To solve these problems, several novel techniques have been proposed and studied theoretically, numerically and experimentally. A review of these techniques has been conducted by Dirker *et al*.[1].

With the recent development of reliable numerical packages and their easy availability, optimisation of coupled convective flow (forced and natural) and conduction heat transfer has become easier to implement, and more popular. A review of the subject has been given by Bejan[4,5], which focuses on the generation of shape and structure in freely morphing convective systems, by maximising global performance subject to global constraints. This view is known as constructal theory. An area where this

theory is of the utmost importance is in heat transfer augmentation[6-9] where volumes reserved for fluids that act as a heating or cooling agent are optimised.

Significant research[10-15] has also been conducted on the flow and heat transfer characteristics of micro-channel heat sinks, because of their promise to cool areas with high heat flux. These studies relied on numerical techniques and experiments[11-19, 27-33] to study the flow and heat transfer characteristics of micro-channel heat sinks.

In the present paper, starting from a basic construction unit (the elemental volume is the constructal approach); we determined numerically the best possible geometry for two types of micro-channel heat sink configurations. The total elemental volume and axial length of the micro-channel heat sink were fixed. We sought to determine the best channel dimensions and system configurations that minimise the peak temperature when the pressure difference across the elemental volume is fixed.

2. MICRO-CHANNEL EMBEDDED INSIDE A HIGH CONDUCTING SOLID

Figure 1a shows a drawing of the physical model and the computational domain for a micro-channel heat sink. Heat is supplied to a highly conductive silicon substrate with known thermal conductivity from a heating area located at the bottom of the heat sink. The heat is then removed by a fluid flowing through a number of micro-channels. Using the advantage of symmetry, we selected for analysis an elemental volume (unit cell) consisting of a micro-channel and the surrounding solid, as is shown in Fig. 1b. This work was based on the model of Qu and Mudawar[12] and Kawano *et al*.[17]

The heat transfer in the elemental volume is a conjugate problem that combines heat conduction in the solid and convective heat transfer in the liquid. The two heat transfer mechanisms are coupled through the continuity of temperature and heat flux at the interface between the fluid and the solid. The fluid with inlet temperature, T_{in} is driven through the micro-channel by a fixed pressure difference $\Delta P = P(z = 0) - P(z = L)$, which is maintained between the channel inlet and outlet. The objective of the following analysis was to determine the heat transfer characteristics for a given micro-channel, and the best possible configuration (L, t_1/t_2, t_2/t_3, H/G) that corresponds to the maximal global thermal conductance, or global minimal thermal resistance.

The following assumptions were made to model the heat transfer and fluid flow in the elemental volume: the hydraulic diameter of the micro-channel under analysis is greater than 10 μm; for water, the continuum regime applies hence the Navier-Stokes and Fourier equations can still be used to describe the transport processes; steady-state conditions for flow and heat transfer; incompressible flow; the properties of the solid and fluid are constant; and the heat transfer due to radiation and natural convection is negligible. It is also assumed that the number of elemental micro-channels is large. Based on these assumptions, the continuity, momentum and energy equations for the cooling fluid were

$$\nabla \left(\rho \vec{U} \right) = 0 \tag{1}$$

$$\rho \left(\vec{U} \cdot \nabla \vec{U} \right) = - \nabla P + \mu \nabla^2 \vec{U} \tag{2}$$

$$\rho C_P \left(\vec{U} \cdot \nabla T \right) = k_f \nabla^2 T \tag{3}$$

where $\nabla^2 = \partial / \partial x^2 + \partial / \partial y^2 + \partial / \partial z^2$, and the origin of the Cartesian frame (x, y, z) is located in the bottom left-hand corner of the computational domain, where $\vec{U}$ is the velocity vector, T is temperature, P is pressure, μ is the viscosity, k_f is the thermal conductivity of the fluid and ρ is the density of the fluid. For the volume occupied by a solid, the momentum equation is simply

$$\vec{U} = 0 \tag{4}$$

and the energy equation is

$$k_s \nabla^2 T = 0 \tag{5}$$

Where k_s is the thermal conductivity of the solids.
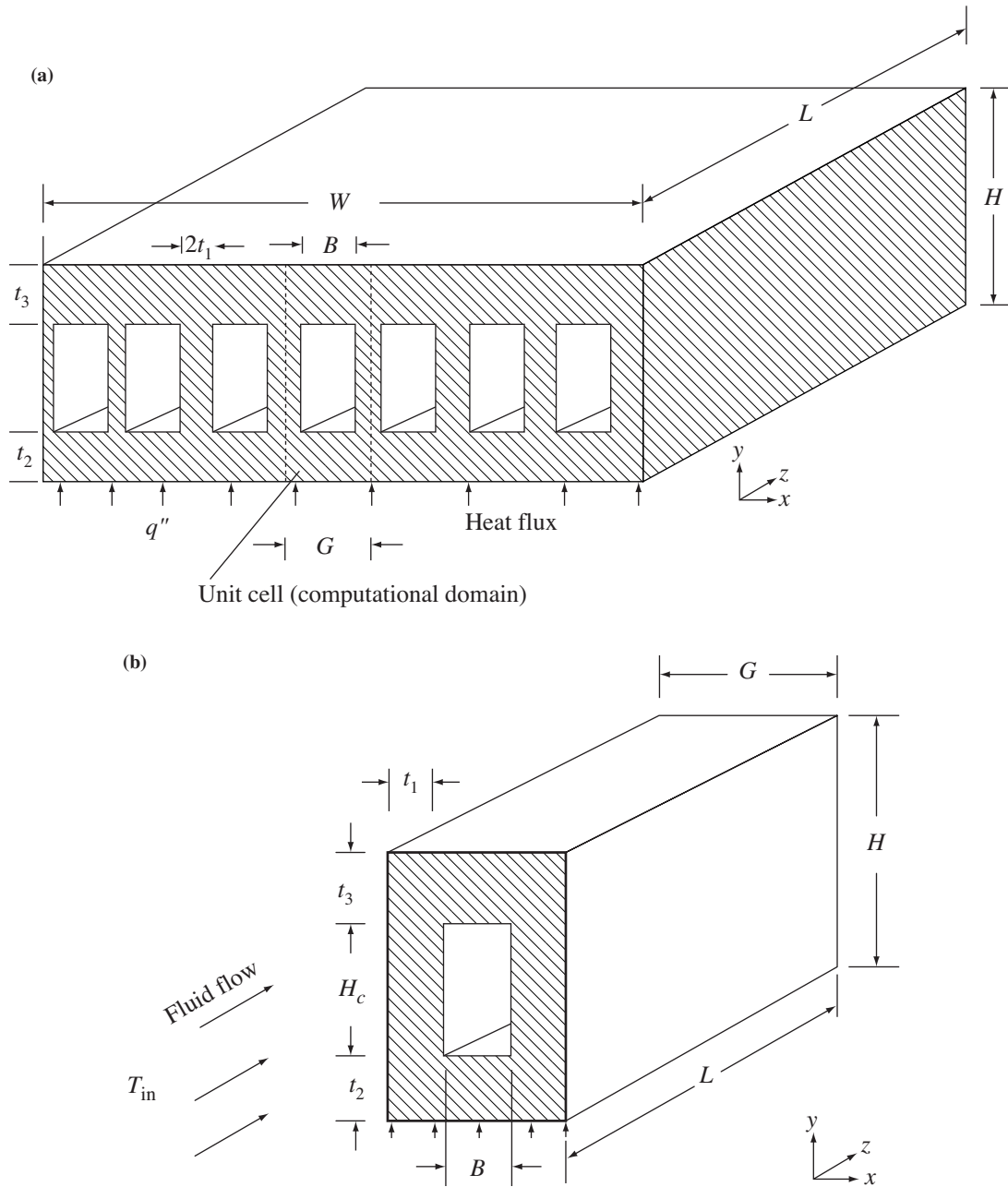
Figure 1. Micro-channel computational unit cell of a heat sink and the computational domain of a micro-channel heat sink.

The entire elemental volume is treated as a continuous domain. The geometric boundary conditions for the computational domains are indicated in Fig. 1b. The flow boundary conditions are such that no-slip occurs on the walls inside the channel. At the entrance of the channel, the pressure boundary conditions become

$$P = \frac{\alpha \mu \, Be}{V^{2/3}} + P_{out} \qquad (6)$$

where Be is the dimensionless pressure drop number based on the elemental volume (the Bejan number, cf. Refs. [20, 21]). $P = 1$ atm, at the channel outlet, and $T = 20°C$ at the channel inlet, V is the volume of the elemental unit. The thermal boundary conditions consist of an assumed uniform heat flux (q'') that is imposed at the bottom of the heat sink

$$k_s \frac{\partial T}{\partial y} = -q'' \tag{7}$$

The remaining outside walls and the plane of symmetry of the heat sink were modelled as adiabatic. The continuity of the temperature and flux at the interface of the solid and fluid surfaces requires

$$-k_s \frac{\partial T_s}{\partial n}\bigg|_\Omega = -k_f \frac{\partial T}{\partial n}\bigg|_\Omega \tag{8}$$

Where, in each case, n is the direction normal to the wall and Ω is the interface fraction of the solid and fluids.

The shapes of the heat sink and cooling channels were allowed to vary, by changing G, H, t_1, t_2 and t_3. We were interested in the geometric configuration that maximises the overall global thermal conductance of the geometry, which in dimensionless form is defined as

$$C = \frac{q''L}{k(T_{max} - T_{in})} \cong \frac{q''L}{k(T_{w,L} - T_{in})} \tag{9}$$

Here q'' is the heat flux from the base of the micro-channel heat sink, k is the thermal conductivity of the fluid, and L is the length of the computational domain of the unit volume. The global conductance C is a dimensionless way of expressing the ratio of the total heat transfer rate q divided by the largest excess temperature $(T_{w,L} - T_0)$ reached at any point in the micro-channel heat sink. The maximum temperature is expected to occur in the exit plane of the micro-channel heat sink. The reciprocal of C is the dimensionless global thermal resistance.

Table 1. Dimensions of micro-channel heat sink Ref. (12).

Case	H/μm	G/μm	t_1/μm	t_2/μm	$(H-(t_2+t_3))$/μm	$(G-2t_1)$/μm	ϕ	L/mm
1	900	100	22.5	270	180	28	0.6638	10

From Table 1, ϕ is the volume fraction of solid materials.

2.1 Numerical Method and Code Validation

The finite volume method was used to solve the continuity, momentum and energy equations. A detailed explanation is given in Patankar[22]. In the finite volume method, the domain is divided into a number of control volumes such that there is one control volume surrounding each grid point. The grid point is located in the centre of the control volume. The governing equation is integrated over each control volume to derive algebraic equations containing a point value of the dependent variable at the grid point. The discretised equations express the conservation principle for a finite volume.

The second order upwind scheme was used to model the combined convection-diffusion effect in the transport equations. The resulting algebraic equations were solved using a line-by-line tri-diagonal matrix inversion algorithm. The SIMPLE algorithm[22] was then applied to solve the coupled systems of equations.

Convergence is obtained when the residuals for the mass and momentum equation are smaller than 10^{-4}, and the residual of the energy equation becomes less than 10^{-9}. A grid-independence test was carried out for the micro-channel heat sink with the dimension given in Table 1. Tests show that a control volume with a mesh size of 25 in the x-direction, 50 in the y-direction and 150 in the z-direction assures a grid independent solution in which the maximum thermal resistance changes less than 2.5% when the mesh is sequentially doubled. This mesh also guaranteed that the numerical results obtained in this work are comparable with predictions and data obtained from experimental and numerical work.

The numerical results generated were compared with the numerical results of Qu and Mudawar[12] for their case when the heating component in Fig. 1 was placed on top of the micro-channel heat sink. Figure 2 compares the thermal resistances, R, for both the inlet and the outlet resistance. The comparison was made using the Reynolds number based on the hydraulic diameter in the range $90 \leq Re_{Dh} \leq 400$. These parameter are defined as

$$R(x) = \frac{T(x) - T_0}{q''} \tag{10}$$
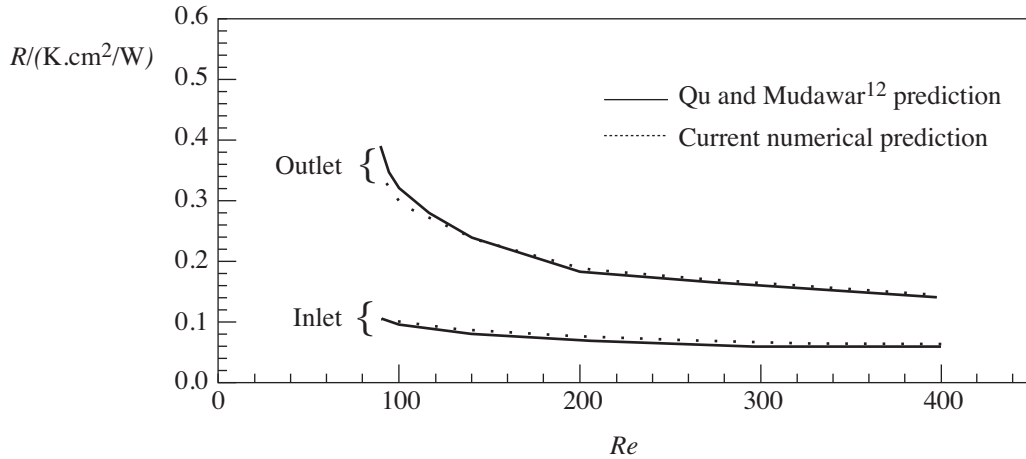
Figure 2. Comparison of numerical predictions at inlet thermal resistance, and outlet thermal resistance.

where x is distance from the entrance, which in this case are located at $x = 0$, and $x = L$. The Reynolds number

$$\text{Re} = \frac{UD_h}{v} \quad (11)$$

From eqn (11), v is the kinematic viscosity, and the hydraulic diameter are

$$D_h \equiv \frac{4A_c}{P_c} = \frac{4BH_c}{2(B + H_c)} = \frac{4(H - (t_2 + t_2)) \times (G - 2t_1)}{2(H + G - (2t_1 + t_2 + t_3))} \quad (12)$$

where A_c is the channel cross-sectional area and P_c is the perimeter of the micro-channel. Figure 2 shows that the present numerical model captures the work of Qu and Mudawar[12], and it predicts very well the inlet and outlet thermal resistances. The maximum difference is 1.8% for the inlet and 1.5% for the outlet. Note also that Qu and Mudawar[12] validated their result by comparing it with the experimental data of Kawano *et al*.[17]

Once the model adopted in this work had been validated, numerical optimisation was conducted to determine the optimal geometry of the micro-channel using the constrained optimisation outlined in the next section. The above code verification and grid-independence test provide confidence in the numerical code used in this work.

2.3. Optimisation Constraints and Parameters

In the present work, we applied constructal theory to an arbitrary unit of a micro-channel heat sink with a fixed given volume (length and cross-sectional area), and substrate material. The only parameter that was allowed to vary is the cross-sectional shape of the micro-channel heat sink, and the ratio of the internal thickness of the vertical and horizontal substrate.

The elemental volume constraint for a given computational cell is

$$GHL = V \text{ (constant)} \quad (13)$$

and the volume of the solid substrate is

$$2Ht_1L + (G\text{-}2t_1)Lt_2 + (G - 2t_1)t_3L = V_s \text{ (constant)} \quad (14)$$

For a fixed length we have,

$$GH = \frac{V}{L} = A \text{ (constant)} \quad (15)$$

The volume of the micro-channel is therefore

$$V_f = V - V_s \text{ (constant)} \tag{16}$$

Equation (14) can also be expressed in terms of the solid volume fraction, $\phi = V_s/V = A_s/A$. Equations (14) – (16) were solved simultaneously for t_1, t_2 and t_3, such that for any changes in the assumed thickness and geometric parameters, the aspect ratios (t_1/t_2, t_2/t_3, H/G and ϕ), the total volume, and volume of solid substrate remain fixed. The volume remains fixed, the cross-sectional shapes of the micro-channel heat sink change in such a way that the solid substrate conducts the heat from the base such that the thermal resistance is minimised. The total number of micro-channels in the micro-channel heat sink arrangement is obtained from

$$num = \frac{W}{B + 2t_1} \tag{17}$$

for a fixed total width, W.

2.4. Scale analysis and the intersection of asymptotic method

In this section, we present the use of a scaling argument to predict the optimal channel geometry that minimises the global thermal resistance or the maximum global thermal conductance. The following assumptions were made throughout the analysis: uniform flow distribution (equal flow in all the channels, constant cross-sectional area of the channels, and no inlet or exit plenum losses), the Prandtl number range $Pr > 0.5$, negligible axial conduction, and the thermal conductivity of the solid substrate being much greater than that of the fluid. The existence of an optimal arrangement can be expected based on the trade-off demonstrated in the forced convection cooling of electronics packages[8], and the method outlined by Muzychka[23]. To determine the optimal channel dimensions, we used the method of intersection of asymptotes[7] for a unit micro-channel as shown in Fig. 2. The global thermal conductance scales were evaluated in two extreme limits (small channel and large channel).

The method of intersection of the asymptotes outlined by Muzychka[23] was used for determining the optimal duct shape. In the limit of small channels, the micro-channel length is covered mainly by fully developed flow and the flow is mainly Hagen-Poiseuille flow, the maximum temperature difference occurs between the outlet wall and the inlet temperature of the micro-channel heat sink. Assuming the total heat generated at the base of the micro-channel is conducted and deposited as heat current at the inner surface of the duct, the total heat transfer for a small duct for fully developed flow gives

$$q_{\text{small}} = \rho A_c U C_p (T_{\text{w,L}} - T_{\text{in}}) \tag{18}$$

C_p is the specific heat of the fluid and U is the average velocity defined as

$$U = \frac{A_c \, \Delta P \, D_h}{\mu \, P_c \, L Po} \tag{19}$$

Po is the Poiseuille number based on hydraulic diameter, and $Po = fRe_{\text{Dh}}/2$, therefore Eqn (18) reduces to

$$q_{\text{small}} = (T_{\text{w},L} - T_{\text{in}}) \frac{\rho C_P A_c^2 \, \Delta P D_h}{\mu P_c L P_O} \tag{20}$$

The resulting expression for the total heat transfer is

$$q_{\text{small}} = k_f (T_{\text{w},L} - T_{\text{in}}) \frac{A_c^2}{P_c} \frac{D_h}{L^3} \frac{Be_L}{P_O} \tag{21}$$

Be_L is the Bejan number based on the channel length ($Be_L = \Delta P L^2/\alpha\mu$). The resulting expression for dimensionless global thermal conductance is

$$C_{\text{small}} = 0.25 \frac{D_h^2}{L V^{1/3}} \frac{Be}{P_O} \tag{22}$$

The above expression shows that for small channels, the dimensionless thermal conductance, C_{small}, is directly proportional to D_h^2.

In the opposite extreme, for large channels, the flow is essentially a boundary-layer flow, and the maximum temperature difference across the thermal boundary-layer is given by

$$q_{large} = \bar{h} L P_c (T_{w,L} - T_{in}) \tag{23}$$

$$\bar{h} L \cong 0.453 k_f \Pr^{1/3} \mathrm{Re}_L^{1/2} \ (0.5 < Pr < 10) \tag{24}$$

where,

$$\mathrm{Re}_L = \frac{U_\infty L}{\nu} \tag{25}$$

The core velocity U_∞ serves as the free-stream velocity for the boundary layer. This velocity follows from the longitudinal pressure force balance on the control volume inscribed inside one channel,

$$\Delta P A_c \cong \bar{\tau} P_c L \tag{26}$$

Where $\bar{\tau}$ is, the mean wall shear stress and is obtained from the boundary-layer solution referenced over the length L

$$\bar{\tau} = 0.664 \rho \, U_\infty^2 \, \mathrm{Re}_L^{-1/2} \tag{27}$$

Finally, combining eqns (25, 26 and 27) yields

$$\mathrm{Re}_L = \left(\frac{\Delta P A_c L}{0.664 \rho \nu^2 P_c} \right)^{2/3} \tag{28}$$

Putting eqn (28) into eqn (23), the total heat transfer becomes

$$q_{large} \cong 0.5192 k_f \left(T_{w,L} - T_{in} \right) \left(\frac{\Delta P A_c P_c^2 L}{\rho \nu^2} \right)^{1/3} \Pr^{1/3} \tag{29}$$

or in terms of Be_L,

$$q_{large} \cong 0.5192 \, k_f \left(T_{w,L} - T_{in} \right) \left(\frac{A_c P_c^2}{L} \right)^{1/3} Be_L^{1/3} \tag{30}$$

In dimensionless form, the global thermal conductance becomes

$$C_{large} = 1.31 \frac{V^{1/9} L^{1/3}}{D_h^{2/3}} Be^{1/3} \tag{31}$$

The above expression shows that, C_{large} is directly proportional to $D_h^{-2/3}$. The dimensionless version of the equations obtained in the two limits, eqns (22 and 31), are reported in Fig. 3. The optimal channel shape can be approximated as the D_h value where the two curves intersect,

$$D_{h,opt} \approx 1.86 \, (L^3 V)^{1/6} Po^{3/8} Be^{-1/4} \tag{32}$$

Po can be approximated using a single-term approximation for the Poiseuille number[24, 25] for $H_c > B$

$$Po = \frac{12}{\left(1 + \dfrac{B}{H_c} \right)^2 \left[1 - \dfrac{192}{\pi^5} \dfrac{B}{H_c} \tanh\left(\dfrac{\pi}{2} \dfrac{H_c}{B} \right) \right]} \tag{33}$$
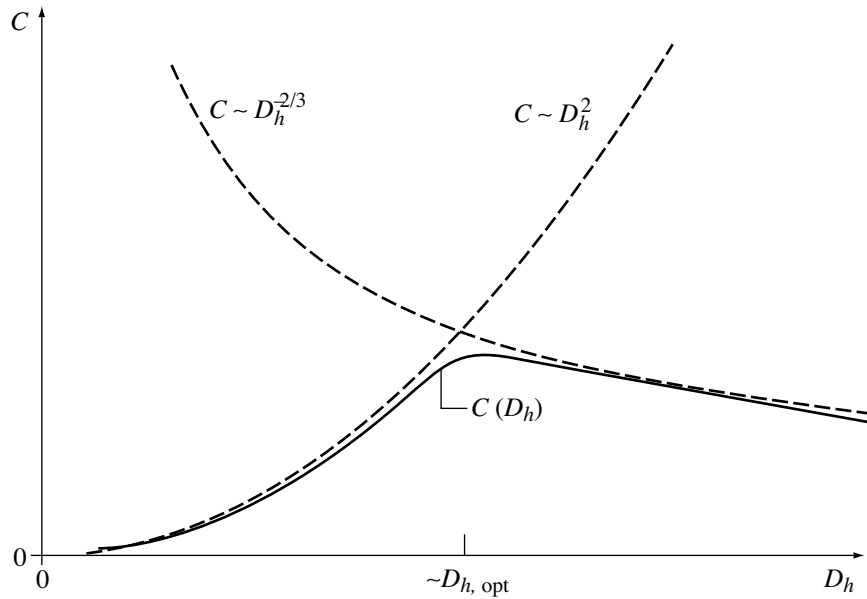
Figure 3. The global thermal conductance in the limit of large channel/duct and small channel and the asymptote method.

Equation (32) can be introduced in eqn (22) or eqn (31) to determine the maximum dimensionless global thermal conductance

$$C_{\max,theoretical} \approx 0.864 \frac{Be^{1/2}}{Po^{1/4}}$$

(34)

As shown above, the intersection of asymptotes method and scale analysis are powerful tools that allow engineers and scientists to estimate trends and optimal configurations [see Ref. [7], preface]. It is important, though, to understand the limits of the theoretical results obtained from eqns (32 and 34). They are only rough estimates of the results and trends. They have to be compared with the results obtained from numerical optimisation. Furthermore, the above relations are valid for large *Be* and according to Knight *et al.*[13], the realistic dimensionless pressure drop number through micro-chips should be typically in the range of 10^8 and 10^{12}.

2.5. Results: Numerical result for optimal geometry for micro-channel heat sinks

In the preceding section, an approximate method was used to determine the optimal channel shape that minimises the global thermal conductance. A series of numerical optimisations and calculations was conducted in this section, and the results are presented in order to show the effects of pressure drop, solid materials and the effect of the external aspect ratio for a fixed set of internal aspect ratios (the ratio of base solid thickness to vertical thickness) on the optimal micro-channel geometry. Some important fluid flow and heat transfer parameters that were employed in this study are summarised in Table 1. The thermophysical properties of water used in this study were based on water at 20 °C. The volume of the micro-channel was fixed and it was based on the data given by Qu and Mudawar[12]. The thermal conductivity of the solid substrate (silicon) was taken to be 148 W/m K. The applied heat flux at the bottom of the micro-channel was fixed at 100 W/cm². We sought to determine the best geometry that minimises the maximum excess temperature, T_{max}, or the overall global conductance.

The micro-channel heat sink has five degrees of freedom, L, H/G, t_1/t_2, t_2/t_3 and ϕ. For this study, three degrees of freedom were fixed L, t_1/t_2 and t_2/t_3, while the other two were allowed to vary with the assumed pressure drop. In the first stage of the optimisation, we fixed the internal structure of the micro-channel by setting ($t_1/t_2 = 0.08$, $t_2/t_3 = 1$ and $\phi = 0.8$). The total volume of the unit micro-channel was set in the range 0.01 mm³ $\leq V \leq 0.9$ mm³, the axial length of the micro-channel was fixed at 10 mm, and

a unit cross-sectional area varied from 0.01 to 0.09 mm^2. The micro-channel heat sink was expected to occupy a total base surface area of 10 mm × 10 mm.

The pressure drop across a unit cell was set at 50 kPa, the total unit volume of 0.9 mm^3 was used for the first optimisation. The aspect ratio (H/G) was optimised for a fixed ϕ. This procedure was repeated for different values of ϕ. Figure 4 suggests that there is an optimal allocation of solid fraction that will minimise the maximum temperatures. At $\phi > 0.6$, the convective resistance increases significantly due to decrease in the hydraulic diameter and hence the fluid becomes overworked. This leads to a jump in the peak temperature, and might account for the behaviour of the curves for $\phi > 0.6$.

Figure 5 summarises the effect of pressure drop on the optimal external aspect ratio, in the range 10 kPa $\leq \Delta P \leq$ 75 kPa. For a fixed solid fraction, the optimal external aspect ratio exhibits two types of behaviour, as shown in Fig. 6. At low pressure drops, the optimised $\left(\dfrac{H}{G}\right)_{opt}$ increases with an increase in the pressure drop, while for $\Delta P \geq 50$ kPa, $\left(\dfrac{H}{G}\right)_{opt}$ increases slightly with increases in the pressure drop, and is almost invariant for $\phi = 0.8$. Similarly, the optimised external aspect ratio $\left(\dfrac{H}{G}\right)_{opt}$ decreases with an increase in the solid volume fraction for the range of geometric parameters used in this study. As the aspect ratio increases, the cross-sectional area of the micro-channel becomes slender in the vertical direction and the value of the hydraulic diameter changes.

Figure 6 shows the behaviour of the optimal micro-channel geometry represented by the optimal hydraulic diameter. $D_{h,opt}$ decreases with an increase in the pressure drop, as suggested from the theoretical derivation of eqn. (32) for a fixed solid volume fraction, and decreases as the volume fraction increases. The minimum optimal hydraulic diameter is more than 100 µm. For the entire range, the optimal hydraulic diameter lies in the continuum region and gives us confidence in our continuum assumption.

Figure 7 describes the behaviour of the minimised maximum temperature difference ΔT_{min} with respect to the applied pressure drop. Note that ΔT_{min} decreases monotonically with increases in pressure
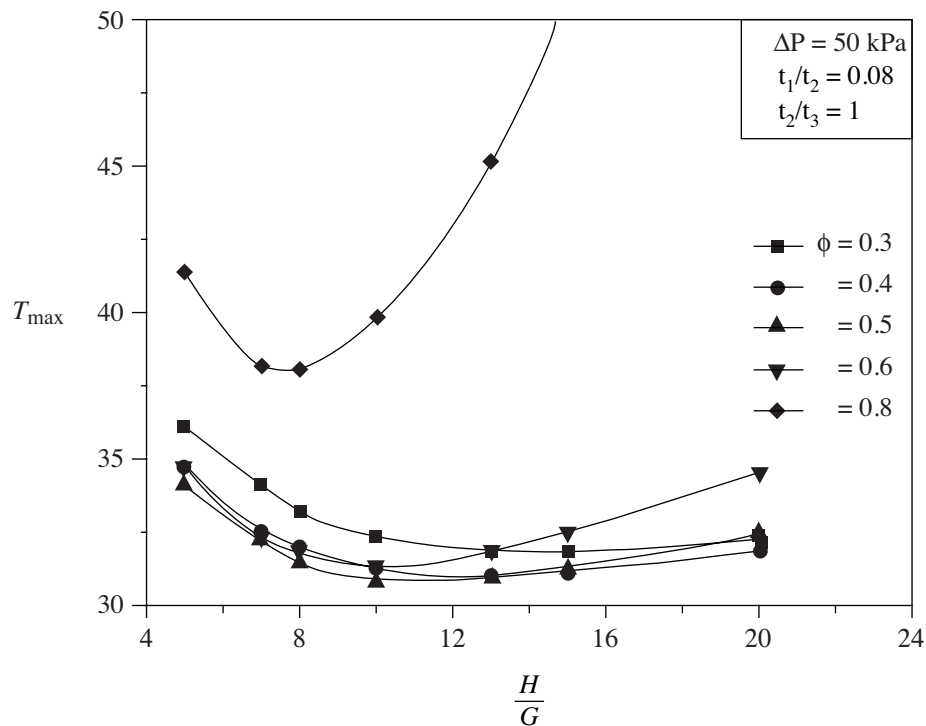
Figure 4. The effects of aspect ratio and solid volume fraction on the maximum temperature.
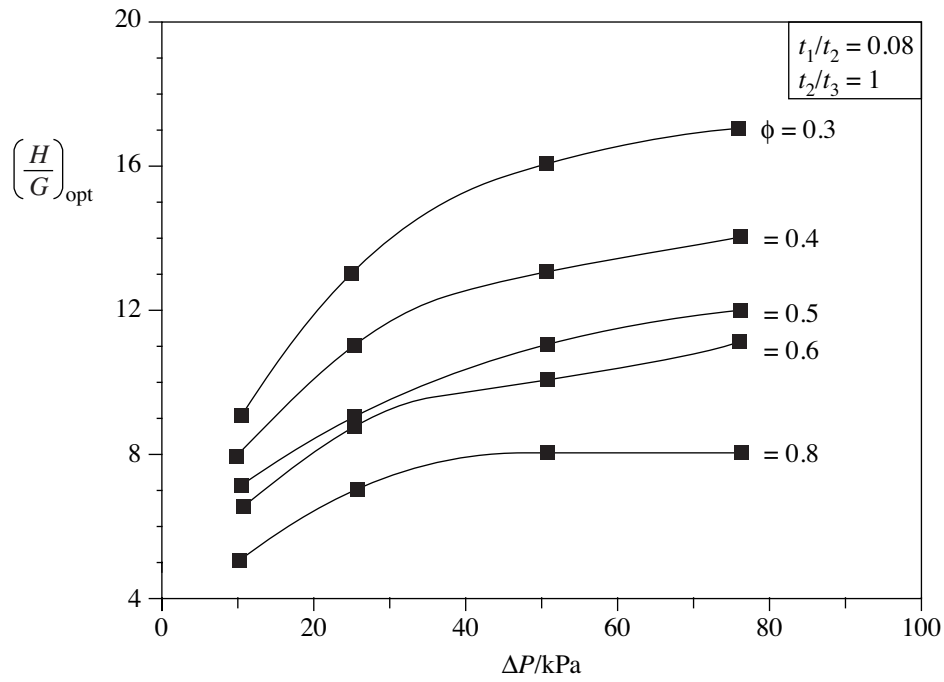
Figure 5. The effect of pressure drop and solid volume fraction on the optimised aspect ratio.
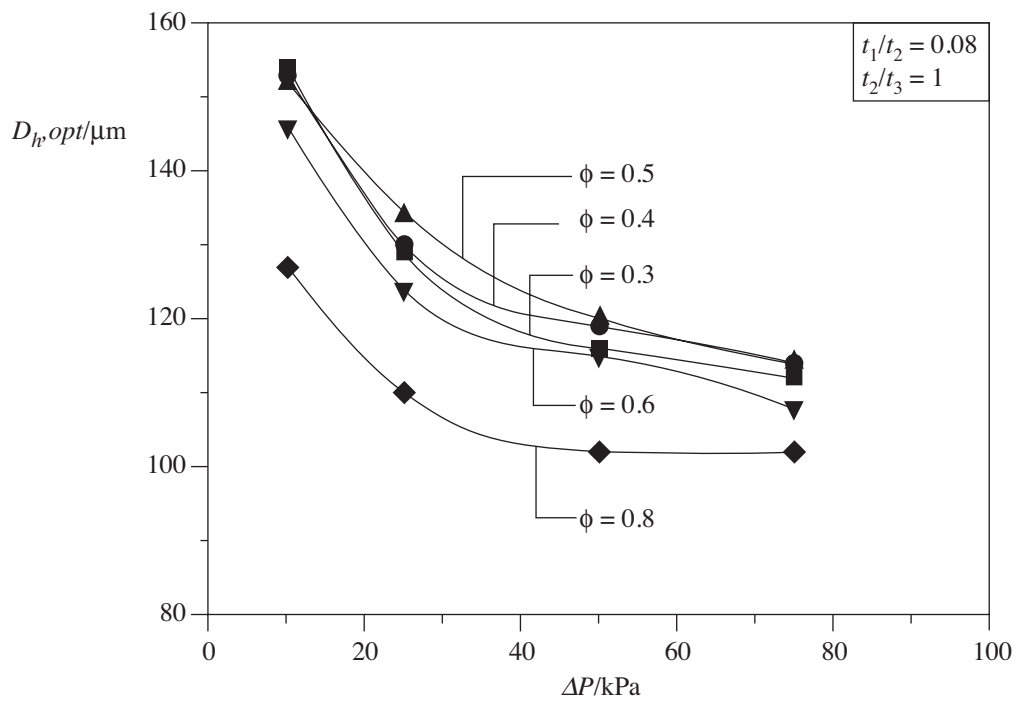
Figure 6. The effect of pressure drop and solid volume fraction on the optimised channel hydraulic diameter.
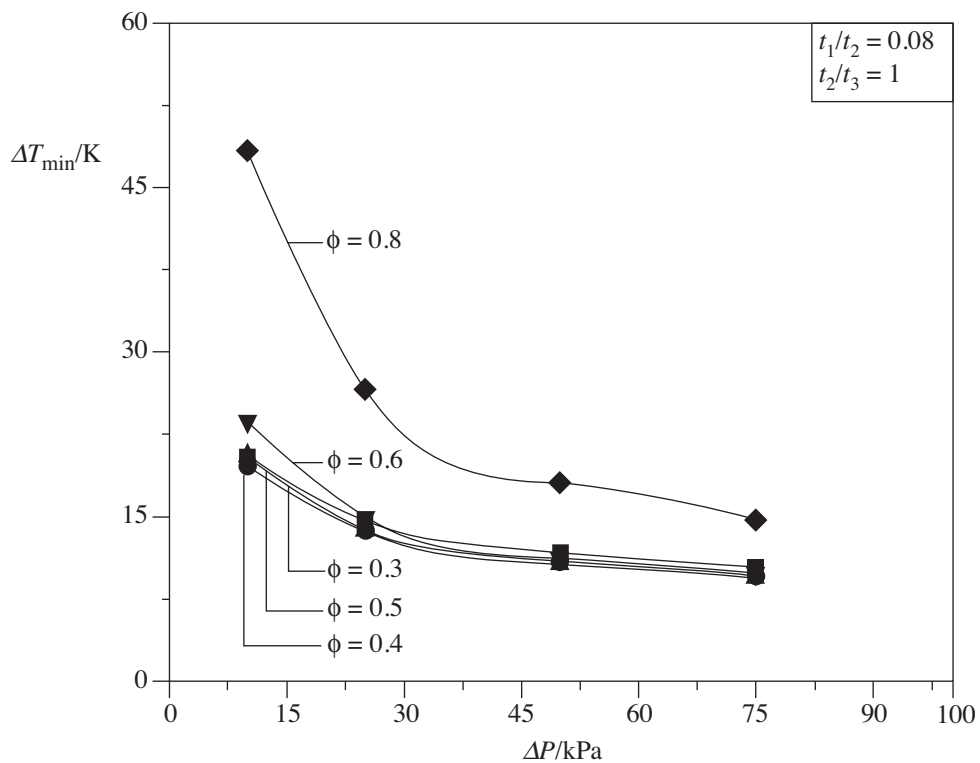
Figure 7. The effect of pressure drop and solid volume fraction on the minimised peak temperature difference.

drop. From Fig. 7, follows that an optimal arrangement of volume of solid fraction exists and lies in the vicinity of $\phi = 0.5$ and 0.4.

For comparison, the scale prediction of Section 2.5 for the maximum heat transfer rate eqn (34) is plotted against the global thermal conductance. The results are reported based on the dimensionless global conductance eqn (9) and dimensionless pressure drop number, Be, eqn (6). The maximised global thermal conductance increases with an increase in Be. For the volume solid fraction, Fig. 8a suggests that an optimal solid fraction exists in the vicinity of $\phi = 0.5$ and 0.4.

Figure 8b shows the comparison between the theoretical solution eqn (34) and the numerical solution. The numerical results follow the trend predicted by eqn (34), but over-predict the numerical
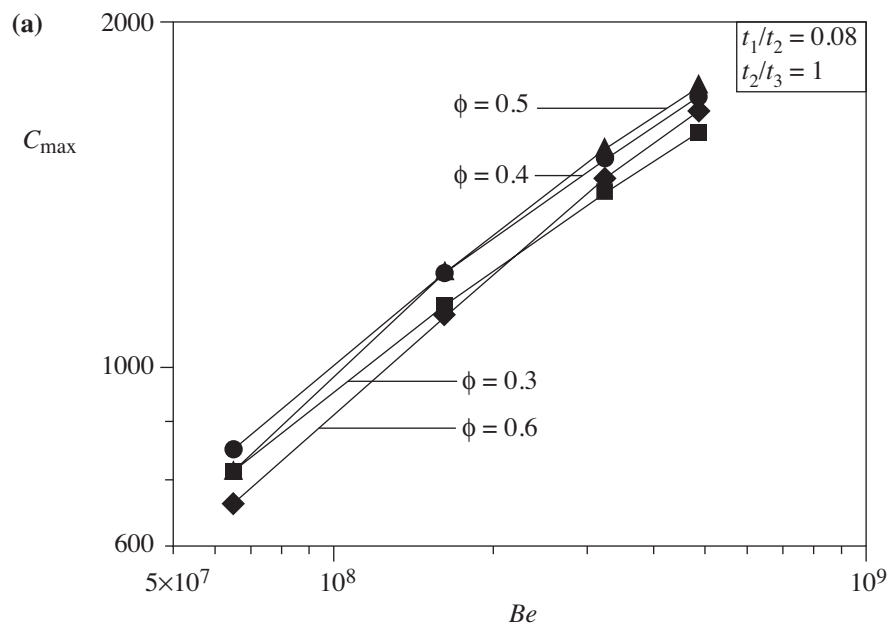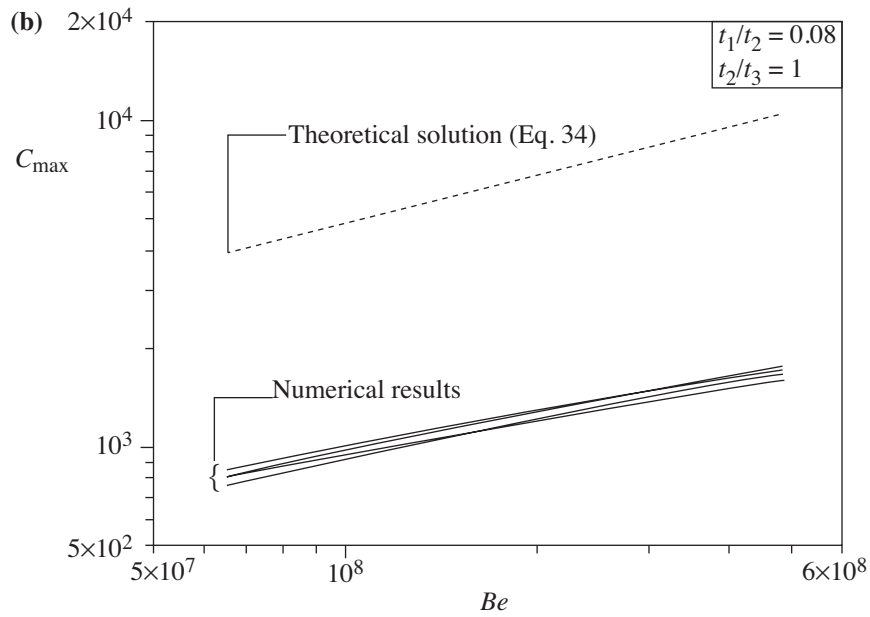
Figure 8. The effect of dimensionless pressure drop number and solid volume fraction on the dimensionless global thermal conductance.

value by a factor of 8, this is due to the simplifying assumptions used in deriving the theoretical solution. For $\phi = 0.5$, the numerical maximised global thermal conductance can be correlated within 0.05% with the power law

$$C_{max} = 0.82 Be^{0.38} \qquad (35)$$

while for eqn (34) and Fig. (11b), the results are represented by the power law

$$C_{max, theory} = 0.6 Be^{0.49} \qquad (36)$$
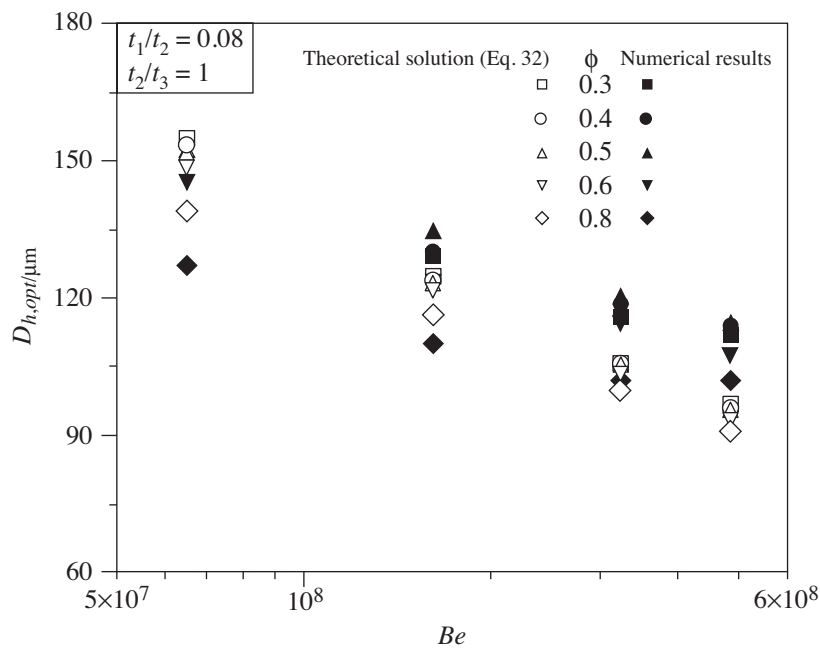
Figure 9. The optimal micro-channel shape (hydraulic diameter) for maximum global conductance.

Figure 9 shows a comparison between the optimal duct shape, $D_{h,opt}$ obtained numerically and the analytical prediction eqn (32). The trend is the same for both solutions. The theoretical and numerical values agree within 1% for the best case, and within less than 10 % for the worst case. These results are in agreement with previous work on the constructal method[5, 19, 23], according to which maximum heat transfer density means optimal packings in which the flow regions that do not contribute to global performance are eliminated.

3. MICRO-CHANNEL EMBEDDED INSIDE A HIGH CONDUCTING MATERIAL AT THE SIDES AND INSULATION COVER ON THE TOP

Figure 10 shows a schematic drawing of the physical model and the computational domain for a heat sink cooling channel capped with a cover plate that is a relatively poor thermal conductor. Heat was supplied to the high conductivity substrate (solid) from a heating area located at the bottom of the heat sink. It was then removed by a fluid flowing through a number of cooling channels, as shown in Figure 10. Using the advantage of symmetry, we selected for analysis a unit cell consisting of a channel and the surrounding solids, as is shown in Figure 10. Attention was focused on the heat transfer optimisation of this unit cell, and the results were extended to the remaining cooling channels.

The heat transfer in the unit cell is a conjugate problem that combines heat conduction in the solid and convective heat transfer in the fluid. The two heat transfer mechanisms were coupled through the continuity of temperature and flux at the interface between the fluid and the solid. The fluid was driven through the channel by a fixed pressure difference $\Delta P = P(z=0) - P(z=L)$, which was maintained between the channel inlet and outlet. This is a good model for electronic systems in which several packages and the channels receive their coolant in parallel from the same plenum. The channel was bathed by a single-phase stream of inlet temperature T_0. The objective of the following analysis was to determine the optimal geometry (L, t_1/t_2, H/G, where G = B/2 + t_1), which correspond to the maximal global thermal conductance. As in other constructal studies, Bejan[4, 27] and Bejan and Almogbel,[27] in present work the search for configuration was subjected to two global constraints:
the elemental total volume constraint for a unit cell,

$$GHL = V \text{ (constant)} \tag{37}$$
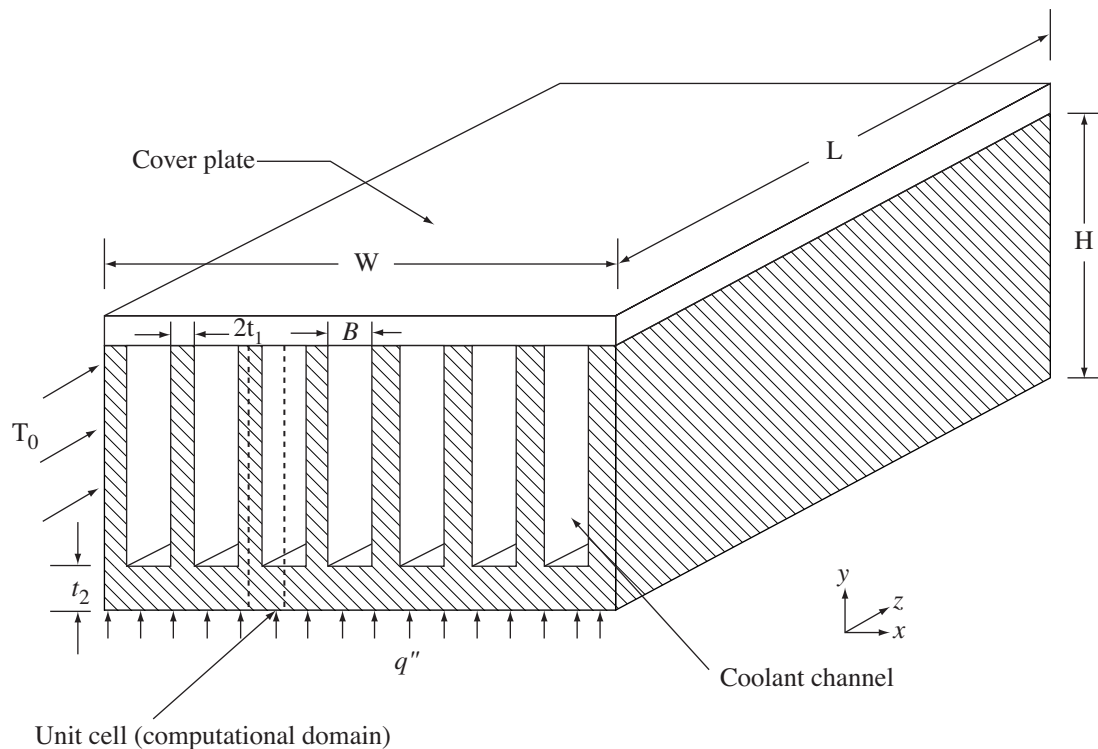
Figure 10. Heat sinks with rectangular cooling channel and the computational unit cell.

and the volume of the solid substrate,

$$(H - t_2)Lt_1 + GLt_2 = V_s \text{ (constant)} \tag{38}$$

The volume of the fluid channel is

$$V_f = V - V_s \text{ (constant)} \tag{39}$$

Equation (39) can also be expressed in terms of the solid volume fraction, $\varphi = V_s/V$.

The following assumptions were made to model the heat transfer and fluid flow in a cell: steady-state conditions for flow and heat transfer; the fluid was incompressible; the properties of the solid and fluid were constant; the heat transfer due to radiation and natural convection was negligible; the number of cooling channels was large; the model chosen for analysis was located at the centre of the heat sink and cooling channel arrangement, hence heat spreading is minimized[11, 28-33].

Equations (1) to (8) and (37) to (39) are non-dimensionalized by using $V^{1/3}$ as the length scale and, $q''V^{1/3}/k$ as the temperature scale. The non-dimensionalisation of the governing equations is achieved by defining the variables

$$(\tilde{x},\tilde{y},\tilde{z},\tilde{L},\tilde{H},\tilde{G},\tilde{t}_1,\tilde{t}_2) = \frac{(x,y,z,L,H,G,t_1,t_2)}{V^{1/3}} \tag{40}$$

$$(\tilde{u},\tilde{v},\tilde{w}) = \frac{(u,v,w)}{\Delta P V^{1/3}/\mu} \tag{41}$$

$$\tilde{T} = \frac{T - T_0}{q''V^{1/3}/k}, \quad \tilde{P} = \frac{P}{\Delta P} \tag{42}$$

The new system is

$$\frac{\partial \tilde{u}}{\partial \tilde{x}} + \frac{\partial \tilde{v}}{\partial \tilde{y}} + \frac{\partial \tilde{w}}{\partial \tilde{z}} = 0 \tag{43}$$

$$\frac{Be}{Pr}\left(\tilde{u}\frac{\partial \tilde{u}}{\partial \tilde{x}} + \tilde{v}\frac{\partial \tilde{u}}{\partial \tilde{y}} + \tilde{w}\frac{\partial \tilde{u}}{\partial \tilde{z}}\right) = -\frac{\partial \tilde{P}}{\partial \tilde{x}} + \nabla^2 \tilde{u} \tag{44}$$

$$\frac{Be}{Pr}\left(\tilde{u}\frac{\partial \tilde{v}}{\partial \tilde{x}} + v\frac{\partial \tilde{v}}{\partial \tilde{y}} + w\frac{\partial \tilde{v}}{\partial \tilde{z}}\right) = -\frac{\partial \tilde{P}}{\partial \tilde{y}} + \nabla^2 \tilde{v} \tag{45}$$

$$\frac{Be}{Pr}\left(\tilde{u}\frac{\partial \tilde{w}}{\partial \tilde{x}} + \tilde{v}\frac{\partial \tilde{w}}{\partial \tilde{y}} + \tilde{w}\frac{\partial \tilde{w}}{\partial \tilde{z}}\right) = -\frac{\partial \tilde{P}}{\partial \tilde{z}} + \nabla^2 \tilde{w} \tag{46}$$

$$Be\left(\tilde{u}\frac{\partial \tilde{T}}{\partial \tilde{x}} + \tilde{v}\frac{\partial \tilde{T}}{\partial \tilde{y}} + \tilde{w}\frac{\partial \tilde{T}}{\partial \tilde{z}}\right) = \nabla^2 \tilde{T} \tag{47}$$

For the volume occupied by solid, the energy equation reduces to

$$\Delta^2 \tilde{T} = 0 \tag{48}$$

The number Be is the dimensionless pressure drop number based on the volume, Be $\Delta PV^{2/3}/\alpha\mu$ (called the Bejan number, cf.[20, 21]). The total volume and solid volume constraints reduce to

$$\tilde{G}\tilde{H}\tilde{L} = 1$$
$$(\tilde{H} - \tilde{t}_2)\tilde{L}\tilde{t}_1 + \tilde{G}\tilde{L}\tilde{t}_2 = \varphi \qquad (49)$$

The entire unit cell was treated as a unitary (continuous) domain. The boundary conditions for the computational domains are indicated in Figures 11b and 11c, where the plastic cover was assumed to have
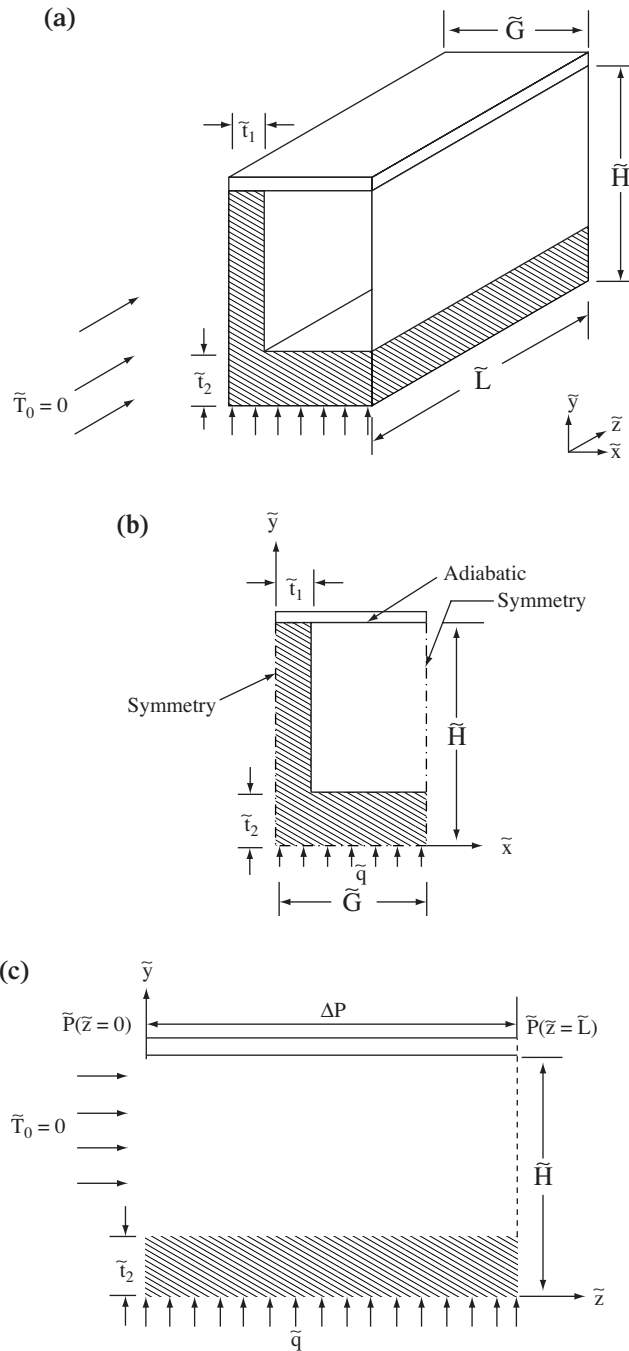
Figure 11. Computational domain of heat sink and a cooling channel with fixed volume and variable shape.

zero thickness. The flow boundary conditions are: no-slip on the walls inside the channel; $\tilde{P} = 1$ at the entrance of the channel, $\tilde{P} = 0$ at the channel outlet, and $\tilde{T} = 0$ at the channel inlet. The thermal boundary conditions consist of a uniform heat flux, $\tilde{q} = 1$, which is imposed at the bottom of the heat sink

$$\tilde{q} = \frac{k(\partial T/\partial n)_{n=0}}{q''} \tag{50}$$

where n is the normal to the walls. The remaining outside walls and the plane of symmetry of the heat sink were modelled as adiabatic. The continuity of the temperature and flux at the interface of the solid and fluid surfaces requires

$$-k_s \left.\frac{\partial \tilde{T}_s}{\partial n}\right|_{\Omega} = -k \left.\frac{\partial \tilde{T}}{\partial n}\right|_{\Omega} \tag{51}$$

where $\tilde{k}$ is the conductivity ratio k_s/k.

The shape of the heat sink and cooling channels was allowed to vary, by changing $\tilde{G}$, $\tilde{H}$, $\tilde{L}$, $\tilde{t}_1$ and $\tilde{t}_2$. Just as in the previous section, we were interested in the geometric arrangement that maximises the overall global thermal conductance of the geometry, which in dimensionless form is defined as

$$C = \frac{q''L}{k(T_{max} - T_0)} = \frac{\tilde{L}}{\tilde{T}_{max}} \tag{52}$$

The dimensionless global conductance measures the quantity of heat flow from the conjugate system per unit temperature between coolant inlet temperature and the peak temperature.

3.1 Optimal Geometry

Using the same numerical procedures as outlined in section 2.1, the micro-channel heat sink structure had three degrees of freedom, $\tilde{L}$, H/G, and t_1/t_2. The values of Be, Pr, $\tilde{k}$ and φ were kept fixed. The search for optimal flow and heat sink configurations was conducted in three nested optimisation loops. First, in the inner loop, we fixed $\tilde{L}$ and H/G and optimised t_1/t_2 such that C reaches a maximum, C_m.

In the next loop, the procedure was repeated for several values of H/G until a family of calculated C maxima revealed a maximum value with respect to having varied t_1/t_2, and H/G, as shown in Fig. 12.
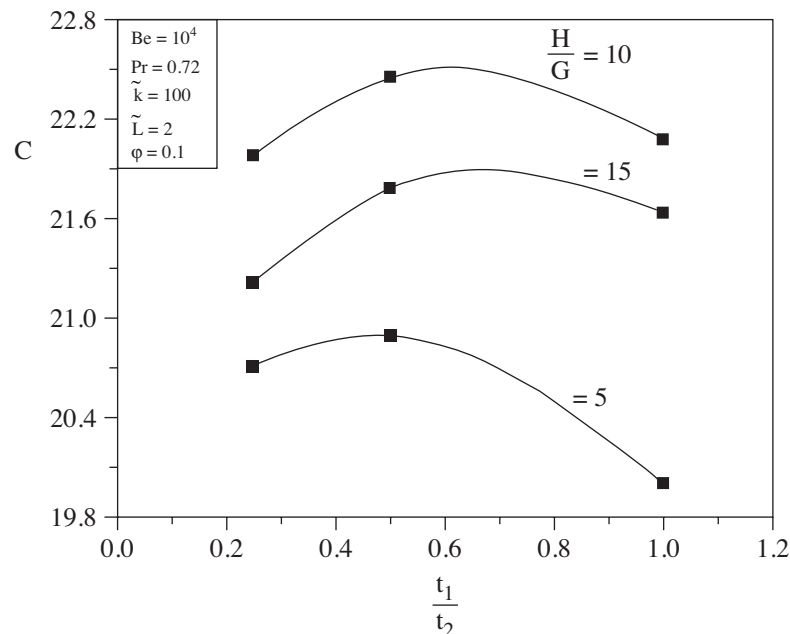
Figure 12. The summary of the maximisation of the global thermal conductance with respect to t_1/t_2 and H/G.

C_{2m} can be maximised with respect to the third free parameter, $\widetilde{L}$. This optimisation constitutes the outermost loop, and its major result is the global thermal conductance C_{3m}. The results of this procedure are the optimised geometry $\widetilde{L}_{opt}$, $(t_1/t_2)_{opt}$ and $(H/G)_{opt}$ and the maximal thermal conductance C_{3m}, which is the largest of the C_m values. These result are functions of the assumed values for Be at fixed φ, k and Pr.

Figure 13 summarises the final stage of the optimisation procedure in the range $10^4 \leq Be \leq 10^6$. This figure shows that the maximum thermal conductance, C_{3m} and the optimal length, $\widetilde{L}_{opt}$, increase with Be. The optimal cross-sectional shape and the shape of the solid component are practically independent of Be, namely $(H/G)_{opt} \cong 7.5$ and $(t_1/t_2)_{opt} \cong 0.75$. From these results, we found that the cross-sectional shape of the cooling channel is also constant, $(H - t_2)/(G - t_1)_{opt} \cong 8.81$. From Figure 14, we concluded that $\widetilde{L}_{opt}$ and C_{3m} vary as

$$\widetilde{L}_{opt} \cong 0.24 Be^{1/4} \tag{53}$$

$$C_{3m} \cong 0.91 Be^{0.35} \tag{54}$$
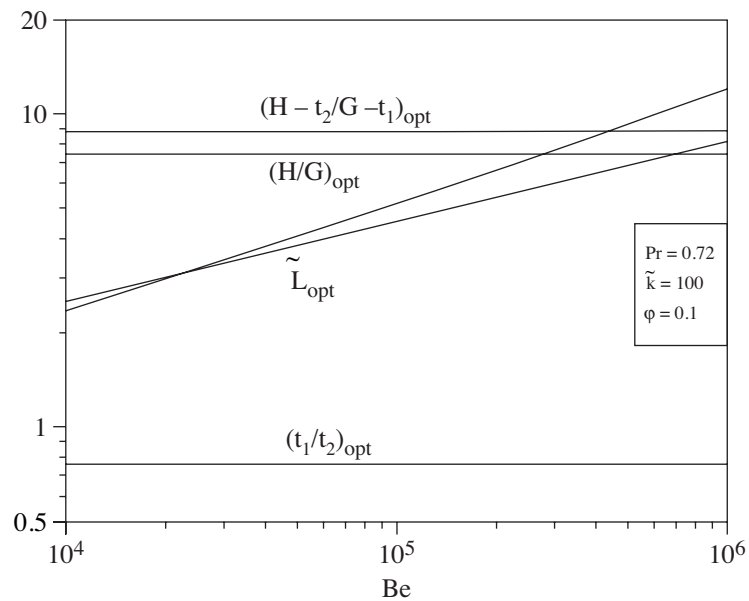
Figure 13. The effect of pressure drop number on the optimised heat sinks and coolant channel.
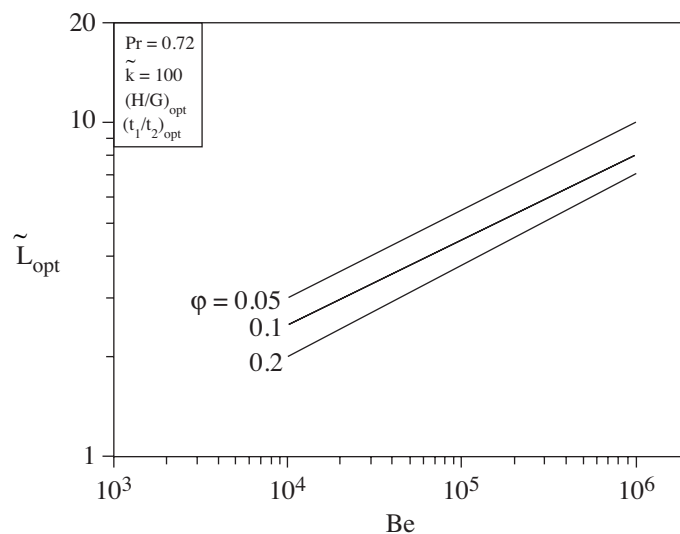
Figure 14. The effect of volume solid fraction and pressure drop number on the optimised longitudinal length.

In view of $(H/G)_{opt} \cong 7.5$ and the volume constraint given in eqn (49), the optimised length shown in eqn (53) is equivalent to an optimal slenderness of the longitudinal profile

$$\left(\frac{L}{H}\right)_{opt} \cong 0.043 Be^{3/8} \tag{55}$$

Eliminating V between eqns (53, 55), the slenderness of the enclosure becomes

$$\left(\frac{L}{H}\right)_{opt} \cong 0.088 Be_L^{1/4} \tag{56}$$

where the number Be_L is based on L, Bejan and Sciubba[9].

$$Be_L = \frac{\Delta P L^2}{\alpha \mu} \tag{57}$$

Note that eqns (53, 55 and 56) have the same form as the relationship obtained for the optimal slenderness of a thin heat-generating strip of width D bathed by a single–phase stream of cold fluid in a duct of fixed volume and longitudinal pressure drop, Bello-Ochende and Bejan[8]. Note further that eqn (56) has a form similar to those obtained for the optimal spacing in stacks of parallel plates with convective heat transfer and fixed volume and pressure drop[30, 33]. Equation (56) proves the importance of Be as the dimensionless parameter in forced convection cooling problems with prescribed longitudinal pressure drop.

Figure 15 shows the effects of the solid volume fraction φ on the optimised longitudinal lengths. It shows that optimised longitudinal length increases with a decrease in φ, and increases as Be increases. In the range $0.05 \leq \varphi \leq 0.2$ and $10^4 \leq Be \leq 10^6$, $\tilde{L}_{opt}$ can be correlated with a standard deviation of 0.00334 by the expression,

$$\tilde{L}_{opt} \cong 0.144 \left(\frac{Be}{\varphi}\right)^{0.25} \tag{58}$$

This correlation has the same form as the theoretical formula obtained by Ordonez[33]. Figure 15 shows the corresponding result for the maximised global conductance. The maximised global conductance increases as the solid fraction increases; this was expected as the available area used for conduction increases.
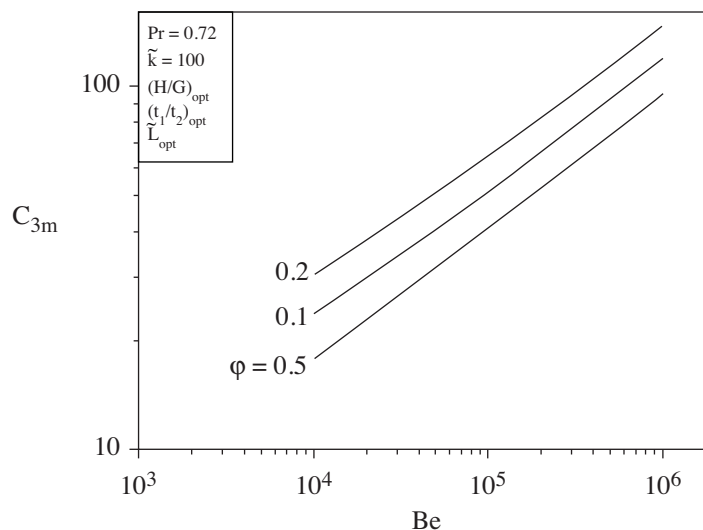
Figure 15. The effect of volume solid fraction and dimensionless drop number on the global thermal conductance.

Next, we considered the important question of the effect of dimensionless thermal conductivity on an optimised structure and its corresponding global thermal conductance. The effect of thermal conductivity on the optimised structure is very interesting: Fig. 16 summarises the effect of $\tilde{k}$ on the maximised global thermal conductance and the optimised structure for a fixed dimensionless pressure drop number, solid volume fraction and Prandtl number. The figure shows that the internal ratio of the conducting solids (heat sink) does not vary much with $\tilde{k}$ and it is approximately $(\tilde{t}_1/\tilde{t}_2)_{opt} = 0.75$. The optimum aspect ratio $(H/G)_{opt}$ increases dramatically with an increase in $\tilde{k}$. This means that the optimised cross-section becomes longer while the optimised longitudinal length $\tilde{L}_{opt}$ becomes shorter. When designing a heat sink cooling channel, the optimised external shape varies for different materials. This is because different materials have different conductivities and the design is not robust relative to the thermal conductivity and varies for different conductivities. As expected, the thrice-maximized global conductance, C_{3m} increases as $\tilde{k}$ increases.

To determine the effect of the Prandtl number on thermal conductance we increased the Prandtl number to 6.2 and repeated the procedure adopted for Pr = 0.72. Figure 17 shows the effect of thermal
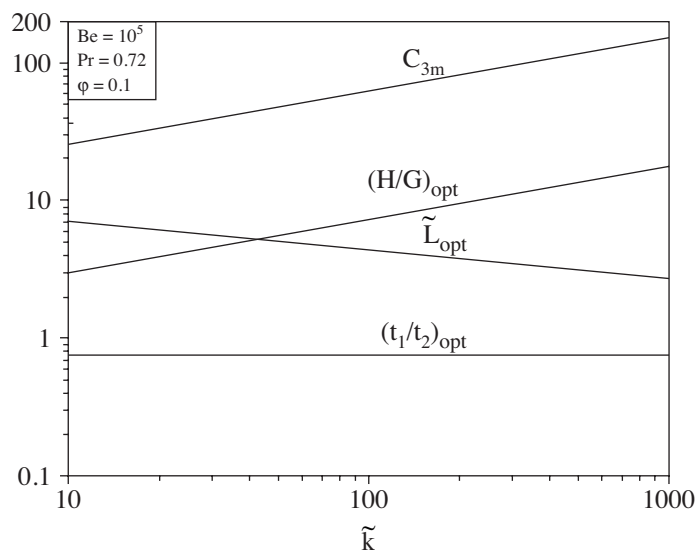
Figure 16. The effect of dimensionless thermal conductivity on the optimised parameters and global thermal conductance.
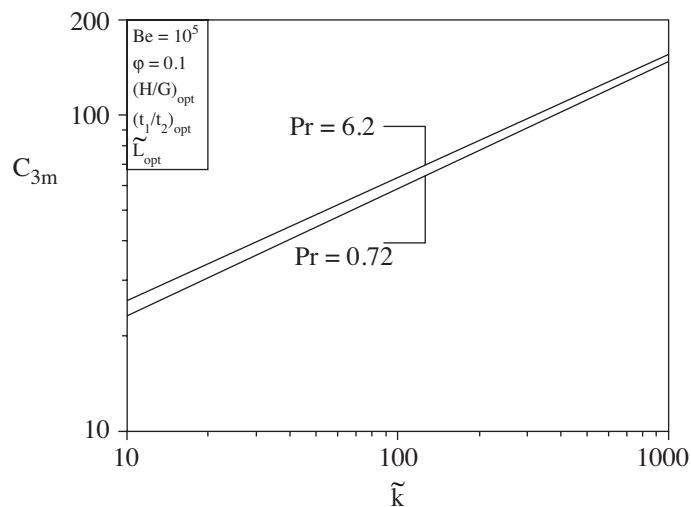
Figure 17. The effect of Prandtl number and dimensionless thermal conductivity on the global thermal conductance.

conductivity and Prandtl number on global thermal conductance. The maximised global conductivity increases with an increase in the Prandtl number, albeit slowly. The optimised structures for Pr = 0.72 and Pr = 6.2 are identical for the range of parameters, and for brevity, the results are not repeated.

The different effects of dimensionless thermal conductivity and dimensionless pressure drop on the optimised structure for a fixed Pr and φ are worth noting. A future challenge is to determine the conjugate system's competitiveness in terms of cost: the cost of pumping the fluid through the cooling channels (pressure drop) and that of using conducting solid with high dimensionless thermal conductivities. The question is which is more profitable, increasing the pumping power or using materials with higher thermal conductivity for a fixed volume, as both increase the global thermal conductance but have different effects on the optimised structure.

3.3 Case Study: Application of Constructal Method to a Micro-Channel Heat Sink

In order to demonstrate the effectiveness of the above method, the constructal method was applied to model studies by Toh et al.[11] and Tuckerman and Pease[10]. The actual dimensions of the micro-channel heat sink and their volume fraction are shown in Table 2; the coolant was water and the conducting solid was silicon wafer with a thermal conductivity of 148 W/m K. The results obtained using the finite volume method are then compared with experimentally measured thermal resistance from different flow rates. The results of this work were then compared with the experimentally measured thermal resistance supplied by Tuckerman and Pease[10] using the local thermal resistance given in eqn (10).

Table 2b reports the maximum thermal resistance for three cases tabulated in Table 2a. These thermal resistances were reported at z = 9 mm. Table 2b shows the comparison between the thermal resistance measured experimentally by Tuckerman and Pease[10] and numerically by Toh et al.[11], and those calculated [using equation (29)] in this study. The agreement with the experimental work is within 28% for case 1, 11% for cases 2 and 3, and with numerical results it is within 3%.

Table 2a. Dimension of the unit cell of a micro-channel heat sink used for the case study
(Toh *et al.*[11], Tuckerman and Pease[10])

Case	H (μm)	G (μm)	t_1 (μm)	t_2 (μm)	H–t_2 (μm)	G–t_1 (μm)	φ	L (mm)
1	533	50	22	213	320	28	0.6638	10
2	430	50	22.5	143	287	27.5	0.633	10
3	458	50	25	156	302	25	0.668	10

Table 2b. Comparison of thermal resistance at x = 9mm.

From Table 2a	q'' (W/cm^2)	Q (cm^3/s)	R(K.cm^2/W)		
			(Tuckerman and Pease[10])	(Toh et al.[11])	Present calculation
			Experimental	Simulation	
1	181	4.7	0.110	0.157	0.154
2	277	6.5	0.113	0.128	0.122
3	790	8.6	0.09	0.105	0.100

The micro-channel heat sink had three degrees of freedom, L, H/G, and t_1/t_2. For the purposes of comparison, one degree of freedom was fixed, L, while the internal structure t_1/t_2 and the external shape were allowed to vary with the assumed pressure drop. The total volume of the unit micro-channel heat sink was fixed at V = 0.215 mm^3, the axial length of the micro-channel was also fixed at 10 mm, and the unit cross-sectional area was 0.0215 mm^2. The micro-channel heat sink was expected to occupy a total base surface area of 10 mm × 10 mm. The pressure drop (gage pressure) across the unit cell was set at 117.2 kPa. The solid material was made of silicon substrate, and the fluid flowing through the channels was water. The thermal conductivity ratio is given as 246.7. Table 3 illustrates the reduction in thermal resistance obtained using the constructal design method. A reduction of 8% in thermal resistance was obtained by varying H/G and t_1/t_2, while keeping L constant for the case given in Table 2.

Table 3. Constructal method for a given micro-channel heat sink arrangement, for case 2 in Table 2.

Pressure drop number (Be = 2.9×10⁸)	8.6	10	15	**20**
$(\widetilde{t}_1/\widetilde{t}_2)_{opt}$	0.16	0.11	0.055	**0.035**
R (x = 1cm, K.cm²/W)	0.122	0.117	0.113	**0.121**
num = $\dfrac{W}{G}$	200	216	264	**305**
Reduction in R (%)	–	4.3	7.6	**0.22**
			OPTIMUM	

CONCLUSIONS

In this paper, we showed numerically and theoretically that the global thermal conductance for two types of micro-channel heat sinks can be maximised by optimising the aspect ratio, *H/G*, the axial length, $\widetilde{L}_{opt}$ and therefore the channel hydraulic diameter for laminar forced-conjugate heat transfer. The micro-channel heat sinks are conjugate problems with conduction in the solid and forced convective flow in the cooling liquid. We started the constructal design of the heat sink cooling channel from an elemental unit cell, and optimised the internal and external structure of the unit cell. This optimal configuration can be further arranged or assembled in a stack to form a larger construct, depending on the required total volume.

Numerical optimisation results further show that the optimal micro-channel shape ($D_{h,opt}$), minimised peak temperature (maximised global thermal conductance), aspect ratio and the axial length are functions of the applied pressure difference and solid volume fraction.

Comparisons of the results obtained numerically with approximate solutions based on scale analysis with those work obtained from literature show excellent agreement for optimal micro-channel dimensions.

It is expected that the conceptual design of micro-channel heat sinks using the constructal method will lead to better and faster design of micro-channel heat sinks with improved performance and higher global thermal conductance (minimised global resistance).

ACKNOWLEDGEMENTS

REFERENCE:

1.   Dirker, J., Liu W., Van Wyk D., Meyer J. P. and Malan A. G., Embedded solid state heat extraction in integrated power electronic modules, *IEEE Transaction on Power Electronics*, 2005, No. 3 20, 694–703.

2   Webb, R., Next generation devices for electronic cooling with heat rejection to the air, *J. Heat Transfer*, 2005, 127, 2–9.

3   Hetsroni, G., Mosyak, A., Pogrebnyak, E. and Yarin, L. P., Heat transfer in micro-channels: Comparison of experiments with theory and numerical results, *Int. J. Heat Mass Transfer,* 2005, 48, 5580–5601.

4   Bejan, A., *Shape and Structure, from Engineering to Nature*, Cambridge University Press, Cambridge, UK, 2000.

5   Bejan, A. and Lorente, S., Constructal theory of generation and configuration in nature and engineering, *Journal of Applied Physics*, 2006, 100, 041301.

6   Bar-Cohen, A. and Rohsenow, W. M., Thermally optimum spacing of vertical, natural convection cooled, parallel plates, *J. Heat Transfer*, 1984, 106, 116–123.

7   Bejan, A., *Convection Heat Transfer*, 3rd edn, Wiley, New York, 2004.

8   Bello-Ochende, T. and Bejan, A., Fitting the duct to the "body" of the convective flow, *Int. J. Heat and Mass Transfer*, 2006, 46, 1693–1701.

9   Bejan, A. and Sciubba, E., The optimal spacing for parallel plates cooled by forced convection, *Int. J. Heat Mass Transfer*, 1992, 35, 3259–3264.

10   Tuckerman, D. B. and Pease, R.F.W., High-performance heat sinking for VLSI, *IEEE Electron*, 1981, Dev. Lett. EDL-2, 126–129.

11   Toh, K. C., Cheng, X. Y. and Chai, J. C., Numerical computation of fluid flow and heat transfer in microchannels, *Int. J. Heat Mass Transfer*, 2002, 45 5133–5141.

12   Qu, W. and Mudawar, I., Analysis of three-dimensional heat transfer in micro-channel heat sinks, *Int. J. Heat Mass Transfer*, 2002, 45, 3973–3985.

13   Knight, R. W., Hall, D. J., Goodling, J. S. and Jaeger C. J., Heat sink optimization with application to microchannels, *IEEE Transaction of Component, Hybrids, and Manufacturing Technology*, 1992, 15 (5), 832–842.

14   Fedorov, A. G. and Viskanta, R., Three-dimensional conjugate heat transfer in the micro-channel heat sink for electronic packaging, *Int. J. Heat Mass Transfer*, 2000, 43, 399–415.

15   Li, J., Peterson, G. P. and Cheng, P., Three-dimensional analysis of heat transfer in a micro-heat sink with single phase flow, *Int. J. Heat Mass Transfer*, 2004, 47, 4215–4231.

16   Tou, S. K. W., Tso, C. P. and Zhang, X., 3-D numerical analysis of natural convective cooling of a 3×3 heater array in rectangular enclosures, *Int. J. Heat Mass Transfer*, 1999, 44, 3231–3244.

17   Kawano, K., Minikami, K., Iwasaki, H. and Ishizuka, M., Micro channel heat exchanger for cooling electrical equipment, Application of Heat Transfer in Equipment, Systems and Education, *ASME HTD*, 1998, 361-3/PID-3, 173–180.

18   Foli, K., Okabe, T., Olhofer, M., Jin, Y. and Sendhoff, B., Optimization of micro heat exchanger: CFD, analytical approach and multi-objective evolutionary algorithms, *Int. J. Heat Mass Transfer*, 2006, 49, 1090–1099.

19   Favre-Marinet, M., Le Person, S. and Bejan, A., Maximum heat transfer rate density in two-dimensional mini-channels and micro-channels, *Microscale Thermophysical Engineering*, 2004, 225–237.

20   Bhattacharjee, S. and Grosshandler, W. L., The formation of wall jet near a high temperature wall under microgravity environment, *ASME HTD*, 1988, 96, 711–716.

21   Petrescu, S., Comments on the optimal spacing of parallel plates cooled by forced convection, *Int. J. Heat Mass Transfer*, 1994, 37, 1283.

22   Patankar, S. V., *Numerical Heat Transfer and Fluid flow*, Hemisphere, New York, 1980.

23   Muzychka, Y. S., Constructal design of forced convection cooled micro-channel heat sinks and exchanger, *In. J. Heat Mass Transfer*, 2005, 48, 3119–3124.

24   Shah, R. K. and London, A. L., *Laminar Flow Forced Convection in Ducts*, Academic Press, NY, 1978, pp. 78–283.

25   Yilmaz, A., Buyukalaca, O. and Yilmaz, T., Optimum shape and dimensions of channel for convective heat transfer in laminar flow at constant wall temperature, *In. J. Heat Mass Transfer*, 2000, 43, 767–775.

26   Bejan, A., *Advanced Engineering Thermodynamics*, 3rd edition, Wiley, New York, 2007.

27   Bejan, A. and Almogbel, M., Constructal T-shape fins, *Int. J. Heat Mass Transfer*, 2000, 43, 2101–2115.

28   Culham, J. R. and Muzychka, Y. S., Optimization of plate fin heat sinks using entropy generation and minimization, *IEEE transaction CPT*, 2001, 24 (2) 159–165.

29   Dirker, J., Van Wyk, J. D. and Meyer J. P., Cooling of Power electronics by embedded solids, *ASME Journal of Electronic Packaging*, 2006, 128, 388–397.

30   Bello-Ochende, T. and Bejan, A., Optimal spacing for mixed convection, *J. Heat Transfer*, 2004, 126, 957–962.

31   Dirker, J., Malan, A. G. and Meyer, J. P., Thermal characteristics of rectangular cooling shapes in solids, *International Journal of Numerical Methods for Heat and Fluid Flow*, 2007, 17 (4), 361–383.

32   Dirker, J. and Meyer, J. P., Heat removal from power electronics in two direction sets using embedded solid state layers–a proposed non-numerical method, *Heat Transfer Engineering*, to appear in, 2009, 30 (5).

33   Ordonez, J. C., Integrative Energy-System Design: *System Structure from Thermodynamic Optimization*. Ph. D. Thesis, Duke University, Durham, NC, ch. 6, 2003.